Theor. Comput. Fluid Dyn.
DOI 10.1007/s00162-009-0143-4

SPECIAL ISSUE ORIGINAL ARTICLE

Ridha Touihri · Azzeddine Soulaimani · Franck Plunian

Stabilized finite element formulation applied to the kinematic Ponomarenko dynamo problem

Received: 25 July 2008 / Accepted: 24 June 2009

Abstract A stabilized finite element (**B**, **q**) formulation is developed to solve the kinematic dynamo problem. As a test case, we solve the induction equation for a given solid body helical flow, embedded in a cylindrical conducting shell. This problem corresponds to the well-known Ponomarenko dynamo. It has the interesting property to have an exact dispersion relation giving the magnetic growth rate as a function of the flow properties. Therefore, it is a good benchmark to test our kinematic dynamo code. We calculated the dynamo threshold and plotted the geometry of the generated magnetic field. We also evaluated the residual error due to our stabilized formulation.

Keywords Magnetohydrodynamics · Finite element · Stabilized formulation · Kinematic dynamo

PACS 47.11.Fg, 47.65.-d, 47.65.Md, 52.30.Cv

1 Introduction

The dynamo effect is a magnetic instability produced by the motion of an electrically conducting fluid [1]. This process is responsible for the existence of the magnetic field in most of the astrophysical objects like planets, stars or galaxies. The geodynamo (in the Earth's liquid core) and the solar dynamo (in the Sun's convection zone) are two examples for which the observations are the most documented [2]. Such a dynamo action has also been investigated in Fast Breeder Reactors [3,4], because of their large dimensions and the high-electrical conductivity of the liquid sodium that they contain. Liquid sodium is also the standard fluid used in the experimental devices aiming at dynamo action or related effects [5].

The numerical counterpart of observations and experiments has led to the development of various codes including those with finite element formulations [6,7]. In previous studies [8,9], we focused on computation of the hydrodynamics in the presence of a strong magnetic field, but at small magnetic Reynolds number Rem. Here, we present the calculation of the magnetic field for a given flow at Rem larger than unity. We use a model

Communicated by O. Zikanov

R. Touihri
Laboratoire de Modélisation Mathématique et Numérique dans les Sciences de l'Ingénieur,
LAMSIN, ENIT, Bp 37, 1006 Tunis le belvédère, Tunisia

A. Soulaimani
Département de Génie Mécanique, ETS, 1100 Notre-Dame O., Montreal, QC H3C 1K3, Canada
E-mail: azzeddine.soulaimani@etsmtl.ca

F. Plunian (✉)
Laboratoire de Géophysique Interne et Tectonophysique, Université Joseph Fourier, CNRS,
Maison des Géosciences, B.P. 53, 38041 Grenoble Cedex 9, France
E-mail: Franck.Plunian@ujf-grenoble.fr

Published online: 12 August 2009

based on a stabilized ($\mathbf{B}$, q) finite element formulation. The main idea is to introduce a scalar quantity q, which, by analogy to the pressure in the incompressible Navier–Stokes equations, acts as a Lagrange multiplier for the magnetic divergence-free constraint. To test our formulation we consider a flow with helical geometry, the so-called Ponomarenko flow [10], which is known to be a dynamo.

The geometry of the Ponomarenko flow corresponds to a cylindrical solid-body helical velocity ($r \leq R_1$) embedded in a stagnant medium ($r \geq R_1$), both parts being electro-conducting. In the original study [10], the geometry is infinite in both directions radial and axial. A magnetic field is generated only if the velocity exceeds some threshold value. It takes the form of a magnetic wave propagating along the axial direction. Given a magnetic wave number k and a magnetic azimuthal mode m, the velocity threshold is shown to depend on the flow geometry and on the magnetic diffusivities of the moving and stagnant parts. Taking a velocity geometry given by $\mathbf{u} = (0, r\omega, \chi\omega R_1)$ (in cylindrical coordinates r, θ, z) and equal diffusivities, the minimum dynamo threshold is obtained for $\chi = 1.3$, $k = 0.39/R_1$ and $m = 1$. This value has been confirmed by various methods [11–13]. We shall test our finite element formulation for this set of parameters. The case of a time-dependent Ponomarenko flow has also been studied [14–16], but will not be considered here.

Because of its rather low value of the dynamo threshold , the Ponomarenko dynamo has been the object of two experimental realizations, one in Riga [17,18] and one in Perm [19,20]. Only the first one has been successful so far, the second one still being under construction. In the Riga device, a counter flow has been added around the inner helical flow in order to obtain an absolute dynamo instability and to keep this way the magnetic field in the device. The corresponding dynamo threshold was found to be slightly higher than the one for the convective instability. In the Perm device, the liquid sodium will circulate in a torus, without counter flow. In this case the expected dynamo will be a traveling wave corresponding to a convective instability. In this paper we shall consider the convective instability of the Ponomarenko dynamo for it is easier to implement than the absolute one and also because it is highly documented. A recent approach based on finite volume has successfully reproduced the absolute instability of the Riga dynamo in both kinematic and dynamical regimes [21–23]. In comparison, our results are more preliminary as we only consider here the kinematic dynamo regime. However, there is no restriction for applying it to the coupled problem.

Finally, it is worth mentioning that the Ponomarenko dynamo has been discussed [24] as a relevant mechanism at the origin of a helical magnetic wave in astrophysical jets as the one measured recently in the center of our Galaxy [25].

2 The (B,q) formulation

The induction equation and the divergence-free constraint are derived from the Maxwell equations in which the displacement currents have been neglected (liquid metal). They are written as

$$\frac{\partial \mathbf{B}}{\partial t} - \nabla \times (\mathbf{u} \times \mathbf{B}) + \eta \nabla \times \nabla \times \mathbf{B} = 0, \quad \nabla \cdot \mathbf{B} = 0, \tag{1}$$

where the magnetic diffusivity is $\eta = 1/\sigma\mu$, σ and μ being the electric conductivity and the magnetic permeability. By analogy to pressure in the incompressible Navier–Stokes equations, we introduce a scalar quantity q which is a Lagrange multiplier for the magnetic divergence-free constraint. It corresponds to adding the term ∇q on the left hand side of the induction equation [8,9]. Using the Galerkin variational formulation, both equations in (1) are multiplied by the weighting functions $\mathbf{B}_\mathbf{h}^*$ and q_h^*, the subscript h denoting a finite element approximation. Then integrating over all the domain Ω, with boundary Γ and where $\mathbf{n}$ denotes the unit vector normal to Γ, the resulting variational problem becomes

$$\begin{aligned}
&\int_\Omega \left[\mathbf{B}_\mathbf{h}^* \cdot \frac{\partial \mathbf{B}_\mathbf{h}}{\partial t} + \eta \, \nabla \mathbf{B}_\mathbf{h}^* \cdot \nabla \mathbf{B}_\mathbf{h} - \mathbf{B}_\mathbf{h}^* \cdot \nabla \times (\mathbf{u} \times \mathbf{B}_\mathbf{h}) \right] \mathrm{d}\Omega \\
&+ \int_\Omega \left[\mathbf{B}_\mathbf{h}^* \cdot \nabla q_h - \eta (\nabla \cdot \mathbf{B}_\mathbf{h}) \, (\nabla \cdot \mathbf{B}_\mathbf{h}^*) + q_h^* (\nabla \cdot \mathbf{B}_\mathbf{h}) \right] \mathrm{d}\Omega \\
&- \int_\Gamma \eta \left[(\mathbf{n} \cdot \nabla \mathbf{B}_\mathbf{h}) \cdot \mathbf{B}_\mathbf{h}^* - (\mathbf{n} \cdot \mathbf{B}_\mathbf{h}^*) \, (\nabla \cdot \mathbf{B}_\mathbf{h}) \right] \mathrm{d}\Gamma \\
&+ \int_\Omega \left[\alpha_1 \nabla q_h \cdot \nabla q_h^* + \alpha_2 (\nabla \cdot \mathbf{B}_\mathbf{h}) (\nabla \cdot \mathbf{B}_\mathbf{h}^*) \right] \mathrm{d}\Omega = 0.
\end{aligned} \tag{2}$$

where the diffusion terms have been integrated by parts. In (2) and throughout the paper, we consider a partition of the domain Ω into elements where piecewise continuous approximations for the independent variables are employed. Tetrahedral elements are chosen in order to be able to mesh any complex geometry.

The originality of our formulation relies on the last two integral terms in (2), which are introduced to stabilize the solution, that is, to avoid appearance of spurious modes (i.e. oscillating solutions). The stabilizing parameter α_1 is a function of the mesh size h and local magnetic Reynolds number

$$\left(Rem_h = \frac{||\mathbf{u}||h}{\eta}\right)$$

and is given by

$$\alpha_1 = \frac{\epsilon_1 h^2 Rem_h}{\sqrt{Rem_h^2 + 4}}.$$

The parameter α_2 is given by

$$\alpha_2 = \epsilon_2 \frac{||\mathbf{u}||h}{2}.$$

The issues of magnetic divergence-free constraint and the convergence with mesh size have already been discussed in [8]. Here we shall study the effect of these two artificial terms on the dynamo threshold and on the divergence-free constraint. Since the Galerkin formulation has been stabilized, provided that we use appropriate values for (ϵ_1, ϵ_2), equal-order linear approximations over tetrahedral elements are used for all variables.

For simplicity we use Dirichlet boundary conditions, the contour integrals in (2) then being dropped. In addition, since the velocity field may not always be continuous in the computational domain, the convection terms in (2) are also integrated by parts. Finally, we obtain a linear system to solve. We use a second-order finite difference scheme. At each time step, the linear system is solved by an iterative GMRES solver and preconditioned by using the ILUT method [9].

3 Numerical results

3.1 Dynamo onset

For our numerical simulations we take $\chi = 1.3$, a domain of height $H = 2\pi/k = 16.11R_1$, with periodic boundary conditions in $z = 0$ and $z = H$. We consider a radius domain $R_2 = 10R_1$ assuming that it is sufficiently large for being compared with the original case for which R_2 is infinite. We use a mesh which is highly refined close to the infinite shear at $r = R_1$ (Fig. 2c). We take an initial condition for the magnetic field of the form

$$\mathbf{B} = (P(r)\cos\theta,\ -(P(r) + rP'(r))\sin\theta,\ P(r)\cos\theta), \qquad \text{with} \quad P(r) = (r - R_2)^2. \tag{3}$$

This field, independent of z, has already a $m = 1$ azimuthal dependence and is divergence-free.

In order to obtain a time-accurate solution, we adopt the usual $GMRES$ iterations convergence criteria that the residual norm must be reduced at least by a factor 10^{-5}. For the $ILUT$ preconditioner we use the following parameters: $nlev = 5$ and $droptol = 5 \cdot 10^{-4}$ (for more details see [26]). We use a mesh containing 33,297 nodes and 158,700 tetrahedrons.

In Fig. 1 the magnetic energy is plotted versus time for several values of the magnetic Reynolds number Rem. Following [11], this dimensionless number is defined as

$$Rem = \frac{R_1 u_{\max}}{\eta} = \frac{R_1^2 \omega}{\eta}\sqrt{1 + \chi^2}. \tag{4}$$

The dimensionless time is expressed in terms of convective timescale $R_1/u_{\max}$. After a transient state for $t \leq 10$ during which magnetic energy decreases, we observe an exponential damping for $Rem \leq 18$ and an exponential growth for $Rem \geq 18.1$ implying that the dynamo threshold is in between. The difference with the

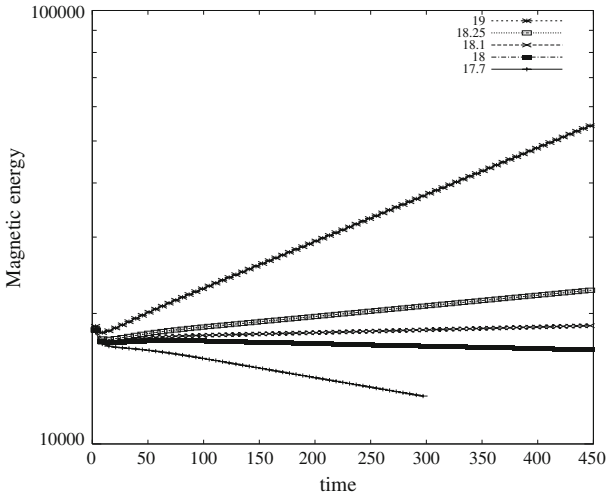

Fig. 1 Magnetic energy versus time for several values of *Rem* indicated by the labels

value 17.7 given in [11] is less than 2.2%. We note that the exponential magnetic energy damping or increase is a direct consequence of the linearity of the induction equation (1). As noted earlier, such an exponential increase is only half of the story as we do not solve here the Navier–Stokes equations with the Lorentz forces. Solving both equations, induction and Navier–Stokes, the kinematic dynamo regime would last only for some time, followed by a saturation of the magnetic energy [22,23].

In Fig. 2 the iso-values of B_z in a (a) radial vertical plane and (b) horizontal plane, show that the generated magnetic field has an azimuthal mode $m = 1$. In (c) we clearly see that the magnetic energy is concentrated in a layer at $r = R_1$, according to the theory [27,28]. In (d) we see that the geometry of the magnetic field has the shape of a double helix. Finally, we found (not shown) that the magnetic field is convected as a wave with a phase velocity in agreement with the one given in [11].

3.2 Effect of numerical stabilization

We tested different values for the couple (ϵ_1, ϵ_2), with $\epsilon_1 \in \{0.1, 1\}$ and $\epsilon_2 \in \{0, 0.1, 1\}$. The residual norm that we obtain is rapidly much lower than 10^{-5} (Fig. 3, left), thus satisfying the convergence criteria for GMRES. Among the different values of (ϵ_1, ϵ_2) that we tested, it turns out that the one $(\epsilon_1, \epsilon_2) = (1, 1)$ corresponds to the one giving the most accurate dynamo threshold. It is also the set of stabilization parameters which is most often used in other cases.

As mentioned earlier, the scalar q in (2) acts as a Lagrange multiplier for the magnetic divergence-free constraint. Not satisfying this constraint would lead to an inaccurate numerical solution. So it is interesting to study how it is affected by stabilization. We calculated $\frac{1}{\Omega}\int_\Omega (\nabla \cdot \mathbf{B})^2 \mathrm{d}\Omega$ at different times (see Fig. 3, right). It keeps decreasing along time, suggesting that it is well satisfied. Again the couple $(\epsilon_1, \epsilon_2) = (1, 1)$ gives the best results.

3.3 Energy balance

Let us introduce the magnetic energy $\mathcal{E}$, the work of the Lorentz forces $\mathcal{L}$, the Joule dissipation $\mathcal{J}$, and the Poynting flux $\mathcal{P}$ defined, respectively, as

$$\begin{aligned} \mathcal{E} &= \int_\Omega \frac{\mathbf{B}^2}{2\mu}\mathrm{d}\Omega, \quad \mathcal{L} = -\int_\Omega (\mathbf{j}\times\mathbf{B})\cdot\mathbf{u}\,\mathrm{d}\Omega, \quad \text{with } \mathbf{j} = \nabla\times\mathbf{B}/\mu, \\ \mathcal{J} &= \int_\Omega \frac{\mathbf{j}^2}{\sigma}\mathrm{d}\Omega, \quad \mathcal{P} = \oint_\Gamma \left(\mathbf{E}\times\frac{\mathbf{B}}{\mu}\right)\cdot\mathbf{n}\mathrm{d}\Gamma \quad \text{with } \mathbf{E} = \eta\nabla\times\mathbf{B} - \mathbf{u}\times\mathbf{B}. \end{aligned} \tag{5}$$

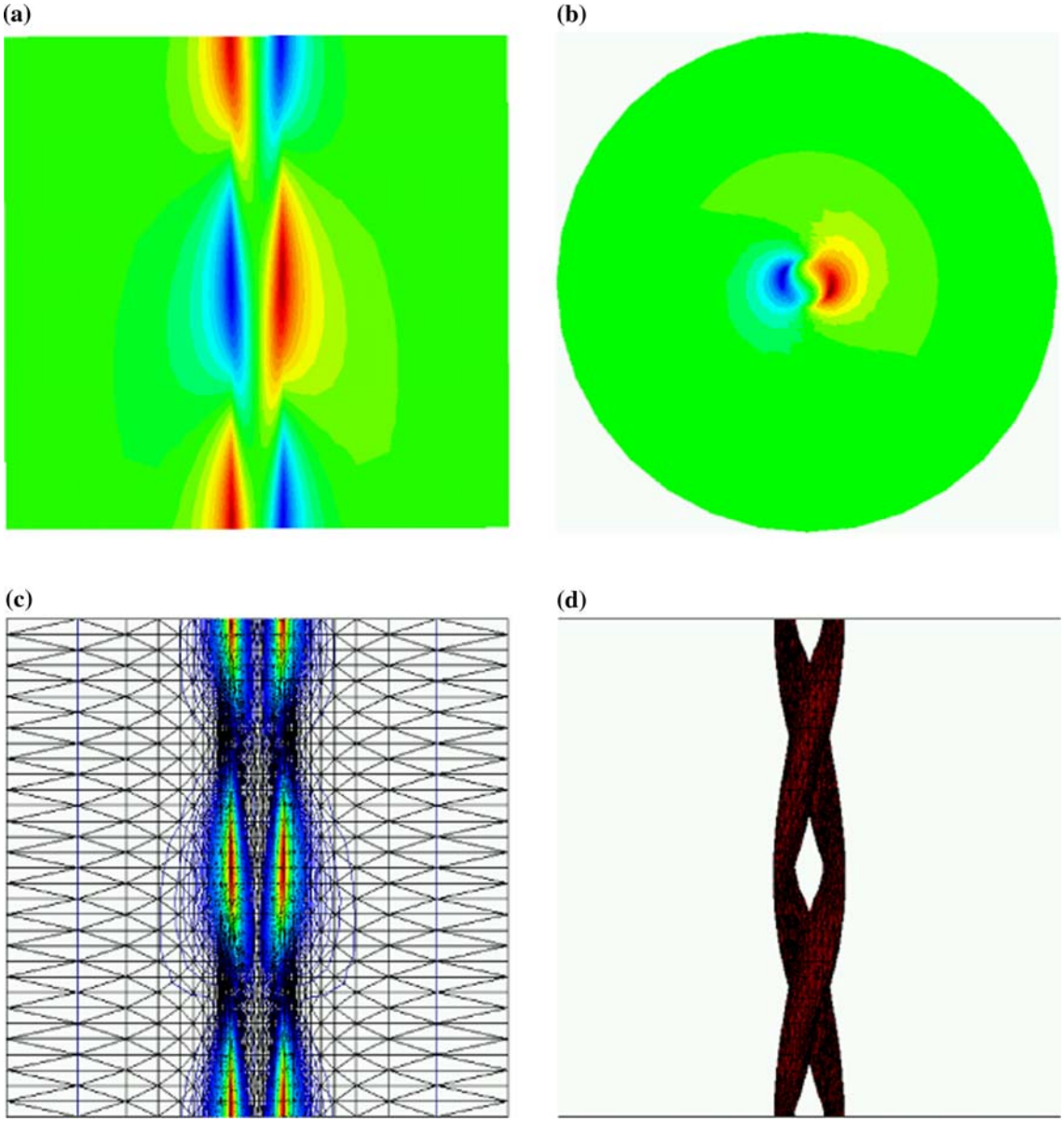

Fig. 2 Iso-values of B_z in a (**a**) radial vertical plane, (**b**) horizontal plane. Iso-values of the magnetic energy in a radial vertical plane (**c**). Three-dimensional iso-surfaces (**d**) of magnetic energy

We find that for each value of Rem, the growth rate γ of the magnetic energy, corresponding to the slopes of the curves plotted in Fig. 1, satisfies

$$\gamma = \partial \ln \mathcal{E}/\partial t = (\mathcal{L} - \mathcal{J} - \mathcal{P})/\mathcal{E}, \tag{6}$$

in agreement with the energetic balance of the induction equation (1). As a consequence, we understand that dynamo action occurs when the work of the Lorentz forces exceeds the sum of the Joule dissipation and the Poynting flux. By definition we have $\mathcal{J} \geq 0$. In addition, we find that $\mathcal{P} \geq 0$ with $\mathcal{P}/\mathcal{L} \approx \mathcal{P}/\mathcal{J} \approx 4.5 \cdot 10^{-3}$ as shown in Fig. 4. This value is rather low though it is not zero. In the original problem [11] to which we compare our results, R_2 is set to infinity implying that $\mathcal{P} = 0$. Therefore, it seems that the accuracy of our results is related to the size of the outer domain to which the Dirichlet boundary conditions are applied. Considering other values of the ratio R_2/R_1, we found that the dynamo threshold is indeed increased for smaller values of R_2/R_1.

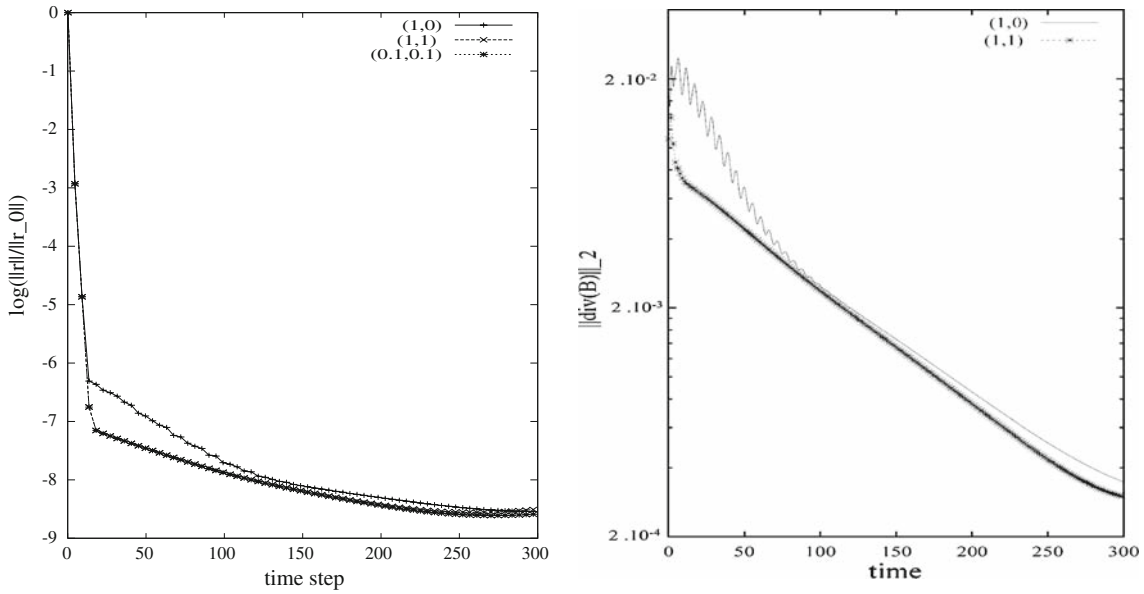

Fig. 3 Residual norm (*left*) and divergence norm (*right*) for $\chi = 1.3$ and $Rem = 25$ for different values of (ϵ_1, ϵ_2) indicated in labels

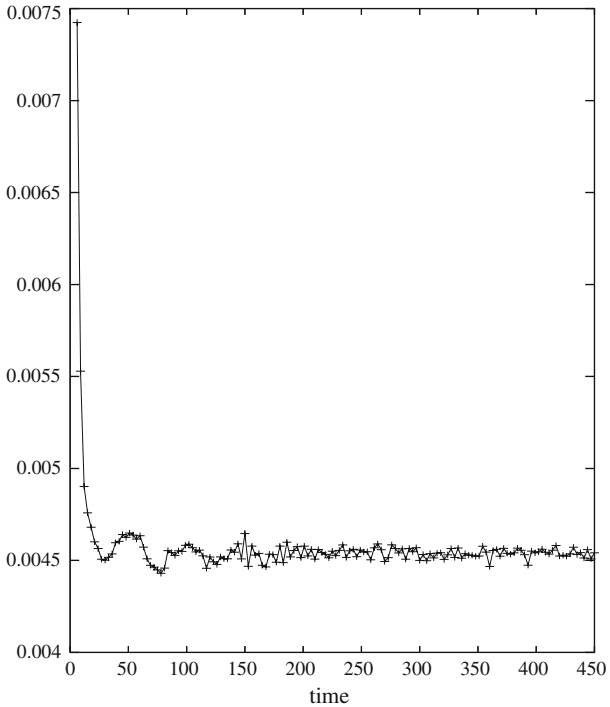

Fig. 4 Time evolution of the ratio $\mathcal{P}/\mathcal{L}$ for $Rem = 25$

4 Conclusion

In this work, we developed a stabilized $(\mathbf{B}, q)$ finite element formulation for the kinematic dynamo problem. An additional function q is introduced in the weak form of the induction equation in order to act by analogy to the pressure in the Navier–Stokes equations, as a Lagrange multiplier for the magnetic divergence-free constraint. We tested our formulation against the Ponomarenko flow. The results show that the additional artificial terms due to the stabilization do not affect the value of the dynamo threshold. The generated magnetic field

corresponds to the one expected by the theory with a concentration of magnetic energy at the cylindrical shear layer, an azimuthal mode $m = 1$, and a non-zero phase velocity. As a continuation of this work, we plan to study the dynamical case in which the magnetic- and flow fields are solved in a coupled way.

Acknowledgments We are grateful to NSERC and University Joseph Fourier which supported visits of RT in Montréal and Grenoble.

References

1. Moffatt, H.K.: Magnetic Field Generation in Electrically Conducting Fluids. Cambridge University press, New York (1978)
2. Dormy, E., Soward, A.M. (eds.): Mathematical Aspects of Natural Dynamos. Taylor & Francis Group, London (2007)
3. Plunian, F., Marty, P., Alemany, A.: Kinematic dynamo action in a network of screw motions. Application to the core of a fast breeder reactor. J. Fluid Mech. **382**, 137–154 (1999)
4. Alemany, A., Marty, P., Plunian, F., Soto, J.: Experimental investigations of dynamo action in the secondary pumps of the FBR superphenix. J. Fluid Mech. **403**, 263–276 (2000)
5. Stefani, F., Gailitis, A., Gerbeth, G.: Magnetohydrodynamic experiments on cosmic magnetic fields. Z. Angew. Math. Mech. **88**, 930–954 (2008)
6. Plunian, F., Massé, Ph.: Couplage magnétohydraulique: modélisation de la dynamo cinématique, in Electromagnétisme et éléments finis, **3**, chapitre 6, 215–247, Hermes (2002)
7. Guermond, J.L., Léorat, J., Nore, C.: A new finite element method for magneto-dynamical problems: two-dimensional results. Eur. J. Mech. B **22**, 555–579 (2003)
8. Ben Salah, N., Soulaimani, A., Habashi, W.G.: A finite element method for magnehydrodynamics. Comput. Methods Appl. Mech. Eng. **190**, 5867–5892 (2001)
9. Soulaimani, A., Ben Salah, N., Saad, Y.: Enhanced GMRES acceleration techniques for some CFD problems. Int. J. Comput. Fluid Dyn. **16**, 1–20 (2002)
10. Ponomarenko, Y.B.: Theory of the hydromagnetic generator. J. Appl. Mech. Tech. Phys. **6**, 755 (1973)
11. Gailitis, A.: The helical MHD dynamo. In: Moffat, H.K., Tsinober, T.S. (eds.) Topological Fluid Mechanics, Proceeding of the IUTAM Symposium, pp. 13–18. Cambridge, August (1989)
12. Marty, P., Ajakh, A., Thess, A.: Magnetic fields in fast breeder reactors: new results on thermoelectricity and dynamo effect. Magnetohydrodynamics **30**, 474 (1995)
13. Avalos-Zuñiga, R., Plunian, F., Gailitis, A.: Influence of electromagnetic boundary conditions onto the onset of dynamo action in laboratory experiments. Phys. Rev. E **68**, 066307 (2003)
14. Normand, C.: Ponomarenko dynamo with time-periodic flow. Phys. Fluids **15**, 1606 (2003)
15. Peyrot, M., Plunian, F., Normand, C.: Parametric instability of the helical dynamo. Phys. Fluids **19**, 054109 (2007)
16. Peyrot, M., Gilbert, A., Plunian, F.: Oscillating Ponomarenko dynamo in the highly conducting limit. Phys. Plasmas **15**, 112104 (2008)
17. Gailitis, A., Lielausis, O., Dementiev, S., Platacis, E., Cifersons, A., Gerbeth, G., Gundrum, Th., Stefani, F., Christen, M., Hänel, H., Will, G.: Detection of a flow induced magnetic field eigenmode in the Riga dynamo facility. Phys. Rev. Lett. **84**, 4365–4368 (2000)
18. Gailitis, A., Lielausis, O., Platacis, E., Dementiev, S., Cifersons, A., Gerbeth, G., Gundrum, Th., Stefani, F., Christen, M., Will, G.: Magnetic field saturation in the Riga dynamo experiment. Phys. Rev. Lett. **86**, 3024–3027 (2001)
19. Frick, P., Noskov, V., Denisov, S., Khripchenko, S., Sokoloff, D., Stepanov, R., Sukhanovsky, A.: Non-stationary screw flow in a toroidal channel: way to a laboratory dynamo experiment. Magnetohydrodynamics **38**, 143–162 (2002)
20. Dobler, W., Frick, P., Stepanov, R.: Screw dynamo in a time-dependent pipe flow. Phys. Rev. E **67**, 056309 (2003)
21. Kenjereš, S., Hanjalić, K., Renaudier, S., Stefani, F., Gerbeth, G., Gailitis, A.: Coupled fluid-flow and magnetic field simulation of the Riga dynamo experiment. Phys. Plasmas **13**, 122308 (2006)
22. Kenjereš, S., Hanjalić, K.: Numerical simulation of a turbulent magnetic dynamo. Phys. Rev. Lett. **98**, 104501 (2007)
23. Kenjereš, S., Hanjalić, K.: Numerical insights into magnetic dynamo action in a turbulent regime. New J. Phys. **9**, 306 (2007)
24. Shukurov, A., Sokoloff, D.D.: Hydromagnetic dynamo in astrophysical jets. In: Krause, F., Radler, K.-H., Rudiger, G. (eds.) The Cosmic Dynamo, pp. 367–371. IAU (1993)
25. Morris, M., Uchida, K., Do, T.: A magnetic torsional wave near the Galactic Center traced by a 'double helix' nebula. Nature **440**, 308–310 (2006)
26. Saad, Y., Soulaimani, A., Touihri, R.: Adapting algebraic recursive multilevel solvers (ARMS) for solving CFD problems. Appl. Numer. Math. **51**, 305–327 (2004)
27. Gilbert, A.D.: Fast dynamo action in the Ponomarenko dynamo. Geophys. Astrophys. Fluid Dyn. **44**, 241–258 (1988)
28. Ruzmaikin, A.A., Sokoloff, D.D., Shukurov, A.M.: Hydromagnetic screw dynamo. J. Fluid Mech. **197**, 39–56 (1988)